ELSEVIER

Journal of Nuclear Materials 301 (2002) 108–117

journal of nuclear materials

www.elsevier.com/locate/jnucmat

The effect of non-metallic inclusions on the fracture toughness master curve in high copper reactor pressure vessel welds

Yong-Jun Oh *, Bong-Sang Lee, Jun-Hwa Hong

Nuclear Materials Technology Development Division, Korea Atomic Energy Research Institute, P.O. Box 105, Yusong, Taejon 305-600, South Korea

Received 27 November 2000; accepted 5 December 2001

Abstract

The fracture toughness of two high copper reactor pressure vessel welds having low upper shelf energy was evaluated in accordance with the master curve method of ASTM E1921. The resultant data were correlated to the metallurgical factors involved in the brittle fracture initiation to provide a metallurgical-based understanding of the master curve. The tests were performed using pre-cracked Charpy V-notched specimens and the master curve was made with an average of T_0 values determined at different temperatures. In all specimens, the cleavage fracture initiated at non-metallic inclusion ranging from 0.7 to 3.5 μm in diameter showing a scatter with the specimens and testing temperatures. Temperature dependency of the triggering particle size was not found. The fracture toughness (K_{J_C}) was inversely proportional to the square root of the triggering inclusion diameter (d_i) at respective temperatures. From this relationship, we determined median K_{J_C} values which correspond to the average value of triggering inclusion diameter of all tested specimens and defined them as a modified median K_{J_C} ($K'_{J_{C(med)}}$). The obtained $K'_{J_{C(med)}}$ values showed quite smaller deviation from the master curve at different temperatures than the experimental median K_{J_C} values. This suggests that the master curve is on the premise of a constant dimension of key microstructural factor in a material regardless of the testing temperature. But the inclusion size at trigger point played an important role in the absolute position of the master curve with temperature and the consequent T_0 value.

PACS: 81.40.Np; 81.70.Bt; 81.05.Bx; 62.20.Mk; 81.20.Vj; 61.72.Qq

1. Introduction

The master curve method, as introduced by Wallin and co-workers, well describes the fracture toughness transition behavior of ferritic steels including reactor pressure vessel (RPV) steels [1,2]. The method is based on Weibull statistical treatment of empirical data and includes the concept of a weakest-link failure for brittle fracture. Large sets of test data accumulated support the validity of the single shape of master curve with temperature, independent of alloy types, provided the material possesses a bcc structure, independent of metallurgical processes and even of irradiation [3–7]. Along with this empirical build-up, there have been efforts to physically rationalize the universal applicability of the single curve shape. Wallin et al. explained it through the similarity between the temperature dependences of plastic energy and fracture toughness ($K_{J_{C(med)}}$) [7]. Natishan, Kirk and Wagenhofer indicated that the short-range barriers for dislocation movement uniquely determine the curve shape and they tried to get the curve

* Corresponding author. Tel.: +82-42 868 8561; fax: +82-42 868 8346.

E-mail address: yjoh@kaeri.re.kr (Y.-J. Oh).

0022-3115/02/$ - see front matter
PII: S0022-3115(02)00716-X

shape through combining the constitutive equation for flow behavior with the plastic work considering the volume over which the work is performed [8–10]. All these empirical confirmations and physical understandings on the single curve shape have been widening the consensus on using master curve technology in the nuclear industry and regulatory bodies.

Meanwhile, as mentioned previously, master curve method includes the concept of the weakest-link failure for brittle fracture that assumes the existence of the microstructural defects such as grain boundary, carbides, inclusions, etc. [1,11–14]. But it has not been clearly explained how the single shape of the master curve is maintained regardless of those microstructural defect variables. An explanation for this issue would provide a profound understanding of the master curve concept in view of the fracture micromechanism and further give a base for dealing with the material uncertainty in the use of the master curve method. Unfortunately, the key microstructural factors controlling fracture process in the transition region are specific to materials and a key factor in a certain material may not operate in another. So, a metallurgy-based understanding of the master curve should be undertaken from a material base.

This paper intends to provide a key microstructural factor involved in the fracture process in the two high copper RPV welds having low upper shelf energy (USE) and correlate it to fracture toughness data and the master curves.

2. Materials and experimental procedure

The materials investigated were WF-233 Linde 80 weld (Mn–Mo–Ni/Linde 80 submerged-arc weld) and the HSST 72 weld, which was primarily made for simulating the low USE Linde 80 welds by the Heavy Section Steel Technology (HSST) program at ORNL. The chemical compositions for the welds are listed in Table 1.

The fracture toughness of the welds was evaluated by the master curve method in accordance with the ASTM standard E1921-97 using pre-cracked Charpy V-notched (PCVN) specimens. The initial crack on the PCVN specimens was located along the weld center-line. The procedure in ASTM E1921 yields a median master fracture toughness curve

$$K_{J_{C(med)}} = 30 + 70\exp(0.019(T - T_0)),$$

where T is temperature and T_0 is a reference temperature.

The master curve incorporates the following relationship on the specimen size effect

$$K_{J_{C(1T)}} = 20 + (K_{J_{C(X)}} - 20)\left(\frac{B_X}{B_{1T}}\right),$$

where $K_{J_{C(X)}}$ and $K_{J_{C(1T)}}$ are the measured toughness values for a given specimen and the equivalent toughness value for 1T size, respectively and B_X and B_{1T} are the thickness values of a given specimen and 1T size, respectively.

Fractography was performed on the fractured specimens using a scanning electron microscope equipped with energy dispersive X-ray spectroscopy (EDS). Quantitative analysis of the inclusions was conducted by measuring the particles on the ductile fracture surfaces, because the inclusions in the voids on the ductile fracture surface reveal their whole appearances while the metallographically polished surface only shows the cut image of the inclusions. The images of ductile fracture surface were taken at a magnification of 2000× and 12 images per each weld were used for particle count.

3. Fracture toughness of the welds

Fig. 1 shows the Charpy impact test curves for 72W and WF-233 welds exhibiting very low upper shelf

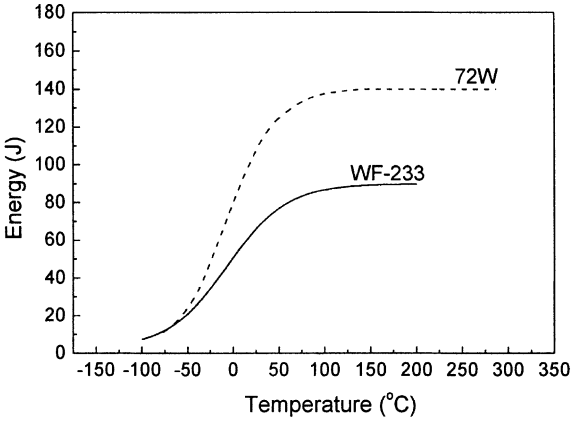

Fig. 1. Charpy curves for the two welds.

Table 1
Chemical compositions of the welds in this study

Welds	Ni	C	P	S	Mn	Si	Mo	Cu
WF-233	0.66	0.076	0.018	0.016	1.60	0.44	0.47	0.22
72W	0.60	0.093	0.006	0.006	1.60	0.44	0.58	0.23

energies. The Charpy index temperatures are similar in the two welds. Fig. 2 represents the $K_{J_C(1T)}$ curves for WF-233 and 72W welds. The resulting reference temperature (T_0) for 72W weld was obtained by averaging the T_0 values at three different testing temperatures of −75, −100 and −120 °C. The T_0 value for WF-233 weld was determined from the data at −90 °C only because of the limited number of specimens. Table 2 lists the T_0 values from the master curve method and the index temperatures from the Charpy impact tests for the two welds. The $T_{41\ J}$ value from the Charpy impact test is higher in WF-233 than 72W, while the T_0 value from the PCVN test is reversed.

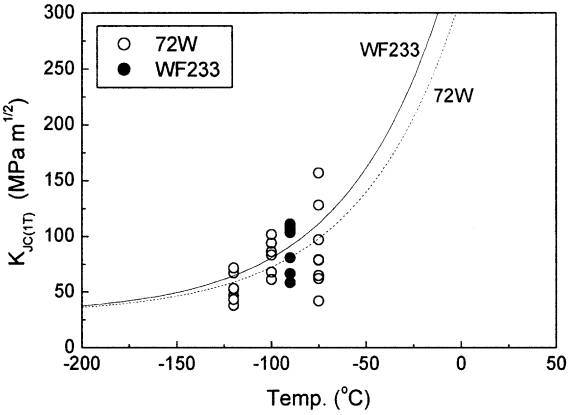

Fig. 2. Fracture toughness test results of the two welds measured by the PCVN specimens.

4. A key metallurgical factor controlling brittle fracture

From the fractography, all specimens in the transition region were found to have a trigger point that initiates brittle fracture and all the trigger points contained inclusions, an example of which is shown in Fig. 3. Fig. 3(c) shows the representative chemical analysis result for

Table 2
The data for fracture toughness test in accordance with ASTM E1921 and Charpy impact test in the two welds

Welds	Testing temperature (°C)	$K_{J_C,med}$ (MPa m$^{1/2}$)	$K_{J_C(1T),med}$ (MPa m$^{1/2}$)	T_0 (°C)	Charpy impact test	
					$T_{41\ J}$ (°C)	USE (J)
72W	−75	110.7	91.9	−68.5	−28	136
	−100	97.5	81.4	−83.7		
	−120	66.0	56.4	−68.7		
Average				−73.6		
WF-233	−90		91.6	−83.0	−15	91

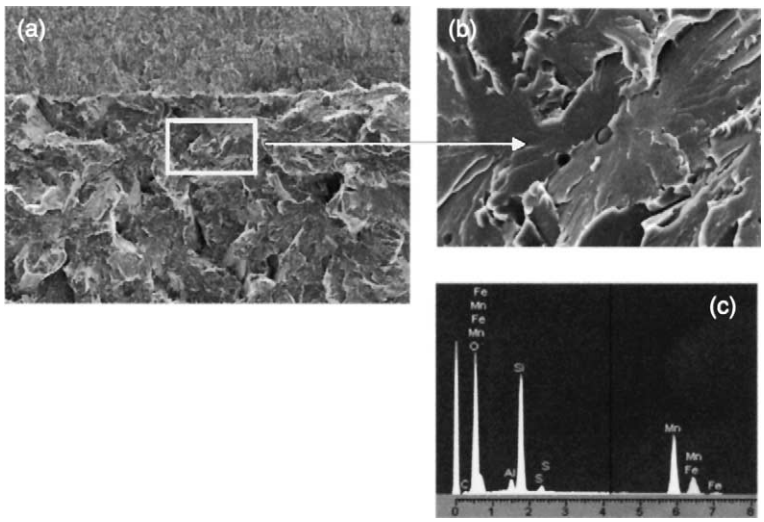

Fig. 3. Fracture surfaces showing brittle fracture initiation at the inclusion ((a) and (b)) and the representative EDS analysis result for the inclusion in WF-233 tested at −90 °C.

the particles using an EDS. Most particles in the two welds were Mn–Si–Al type inclusions containing O and S, which is consistent with the reports by Lawless [15, 16]. Figs. 4 and 5 show the inclusions located at the trigger points of all PCVN specimens tested in this study. Regarding the weakest link failure theory governing brittle fracture, this finding confirms that the key microstructural factor determining fracture toughness in these welds should be the inclusion. Fig. 6 represents the measured inclusion size at the trigger points with the testing temperature. Although the value is lower at the middle testing temperature of −100 °C than the others, the temperature dependency of the triggering inclusion size is not totally found.

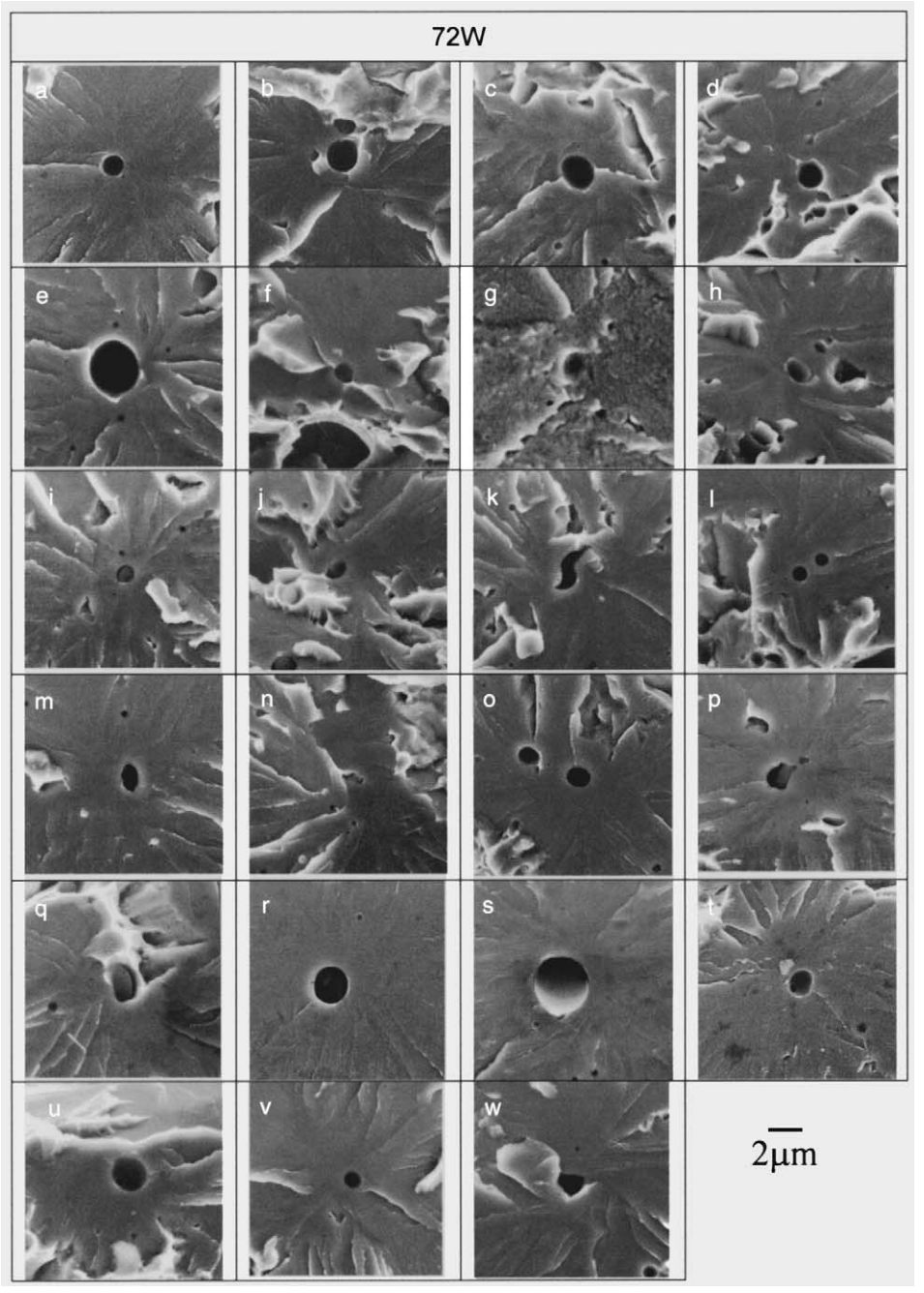

Fig. 4. The inclusions at trigger points in the specimens of 72W weld (a–i: −120 °C; j–o: −100 °C; p–w: −75 °C).

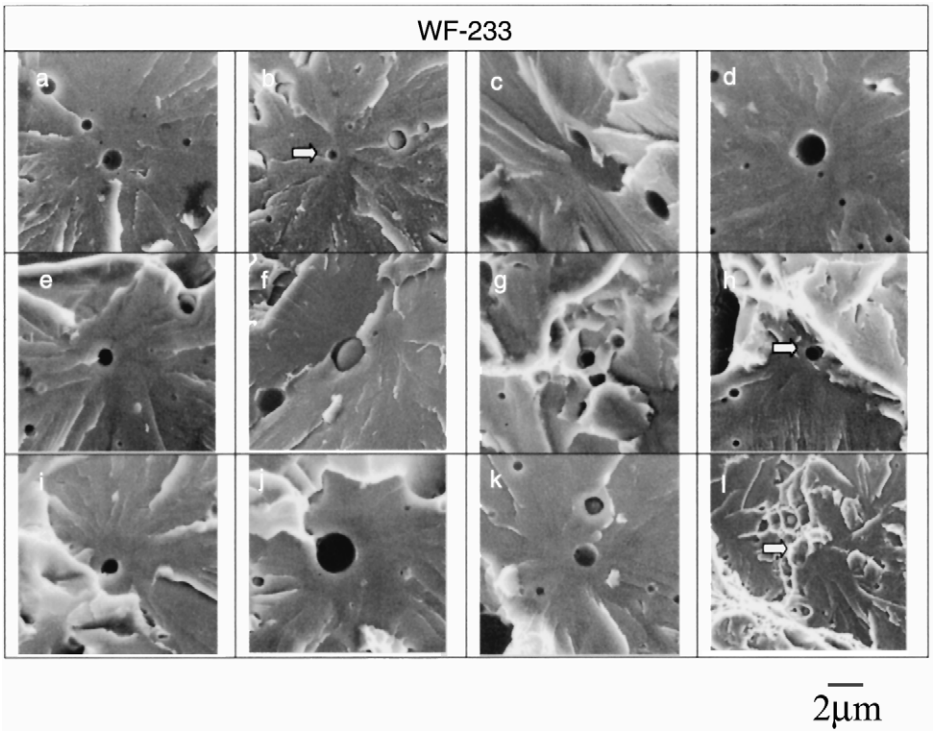

Fig. 5. The inclusions at trigger points in the specimens of WF-233 weld (a: −140 °C, b: −120 °C, c–i: −90 °C, j–k: −75 °C, l: −60 °C).

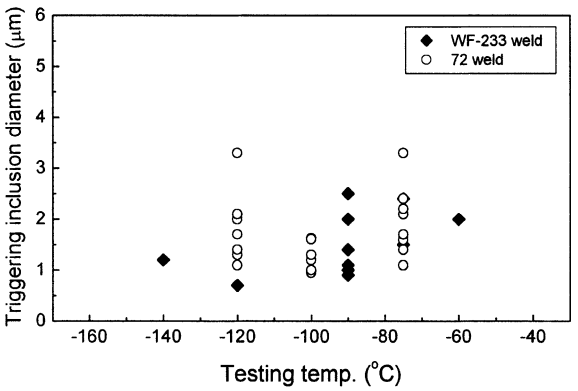

Fig. 6. Inclusion diameter with respect to the testing temperature for the two welds.

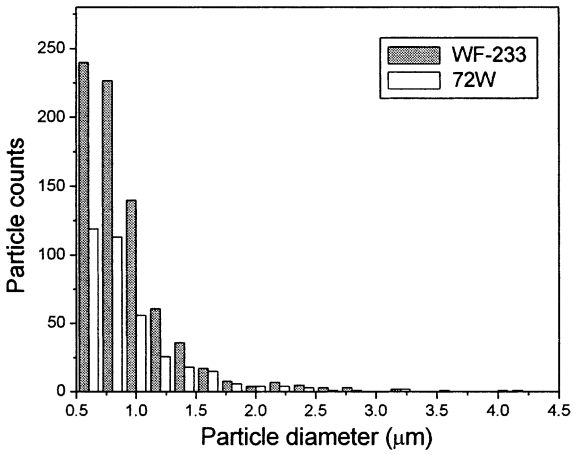

Fig. 7. The inclusion size distribution in the two welds.

The total (global) inclusion size distributions in the two welds are given in Fig. 7. The population in the WF-233 weld is higher than 72W weld, but becomes similar in the size range of over 1.5 μm. On the other hand, the relative frequency of the inclusion size found at the trigger point of the PCVN specimens is plotted in Fig. 8. The frequency distributions in the two welds are interestingly quite similar in spite of the large difference in the total inclusion size distribution. From these two figures, the susceptibility for fracture ($P_{f(i)}$) of each inclusion sized within a certain range (i) can be obtained by dividing the relative frequency of the triggering inclusions in that size range by the relative amount of the total inclusion per unit volume in that range

$$P_{f(i)} = \frac{S_{t(i)}/N_i}{\sum_{i=1}^{n}(S_{t(i)}/N_i)},$$

where $S_{t(i)}$ is the relative frequency of triggering inclusions sized in an i-range and N_i is the ratio of the

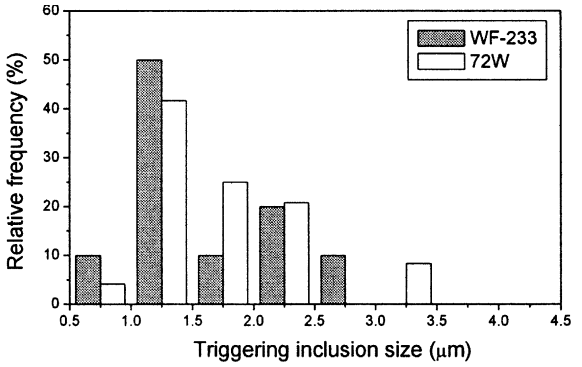

Fig. 8. The relative frequency of triggering inclusion with respect to the size.

inclusions sized in the i-range to the number of the total inclusions per unit volume. Fig. 9 shows the plot of $P_{f(i)}$ as a function of the inclusion diameter. It linearly increases with the inclusion diameter beyond a certain critical size. This means that a tendency toward fracture of each inclusion increases with size. But Fig. 8 shows that the frequency of triggering inclusions decreases with size after some maximum point. This can be explained by supposing a critical or optimum volume in front of crack-tip to initiate a cleavage fracture that has been mentioned by many researchers [17–19]. If the number of inclusions drops off rapidly with inclusion size, then no large inclusion may be available to initiate fracture in the critical volume. We do not go into further detail about this at the present work, but further work would enable quantitative determination of the crack-tip critical volume for brittle fracture related to the inclusion distribution.

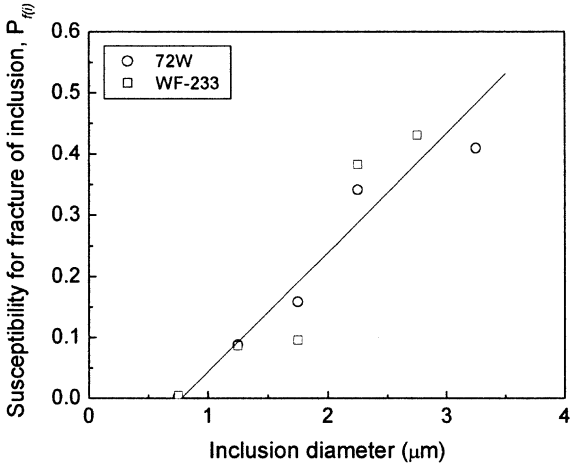

Fig. 9. The change of the susceptibility for fracture of the inclusion with respect to the size.

5. Relationship between inclusion and the master curve

When the tests are performed at different temperatures, different T_0 values may be obtained at each temperature. In this case, based on the ASTM E1921 standard procedure, the average value of all measured T_0s is determined as the reference temperature of the material. Fig. 2 presents the master curve for the average T_0 value and the K_{J_C} values at the three testing temperatures. The difference among the T_0 values obtained at the respective testing temperatures was about 15 °C. The deviation might fall in the general scattering range in large data set. However, regardless of whether the deviation is the generic data scatter or not, the assessment of this deviation in relation to the microstructure would provide a clue to understanding how metallurgical factors affect the master curve.

In the preceding section we suggested that the key microstructural factor in the high copper Linde 80 type welds was the inclusion. Fig. 10 shows the K_{J_C} as a function of the triggering inclusion size for all tested specimens. There exists a meaningful relationship between the inclusion size and fracture toughness and interestingly the slope of the curves of the K_{J_C} versus $\sqrt{1/d_i}$ was quite similar in spite of the different testing temperatures and materials. The fitting lines in Fig. 10 were drawn with a common slope of all data, passing through the point positioned by the $K_{J_C(\mathrm{med})}$ and $\sqrt{1/d_{i(\mathrm{med})}}$ at respective temperatures where $d_{i(\mathrm{med})}$ is the median diameter of the triggering inclusions in the specimens tested at the same temperature. As already indicated in Section 4 referring to Fig. 6, it was uncertain whether triggering inclusion size depends on the testing temperature or not. So, in the present work, with the assumption of a constant triggering inclusion size independent of the testing temperature, we newly determined $K_{J_C(\mathrm{med})}$ values corresponding to the average value of

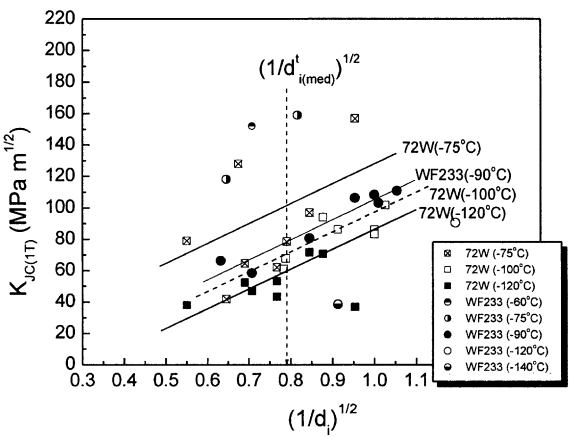

Fig. 10. Fracture toughness versus inclusion size at trigger points.

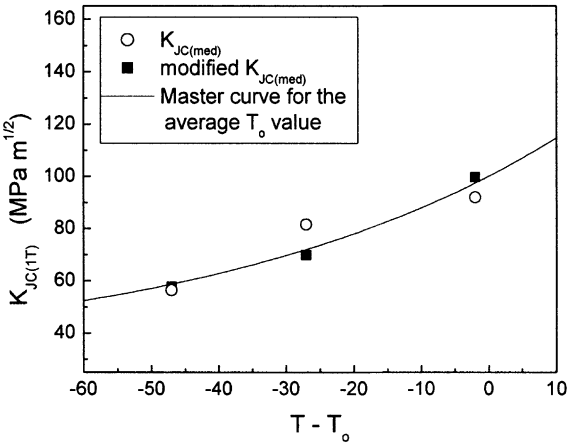

Fig. 11. A comparison of the median fracture toughness values with and without modification by the triggering inclusion size.

$d_{i(\mathrm{med})}$ at all testing temperatures ($d^{t}_{i(\mathrm{med})}$) from the relationship in Fig. 10. This process may eliminate the effect of the triggering inclusion size on fracture toughness of the material. Fig. 11 compares the newly determined $K_{J_C(\mathrm{med})}$ values through this procedure with the original $K_{J_C(\mathrm{med})}$ values in the 72W weld. The new values well match with the master curve, showing quite smaller deviation from the master curve than before at three testing temperatures. This suggests that the single master curve shape is on the premise of a constant dimension of key microstructural factor in a material regardless of the testing temperature. In other words, the key microstructural factor can vary with material, but as far as its dependency on the temperature does not exist, it would not have influence on the single shape of the master curve. This finding confirms the idea of Natishan et al. that the temperature dependency of the master curve depends only on the short-range barriers to dislocation motion in the atomic scale but not on the athermal long-range barriers including inclusion in this work [9,10].

On the other hand, the inclusion size at the trigger point played an important role in the absolute position of the master curve with temperature and the consequent T_0 value. Fig. 12 shows an evident relationship between T_0 values and the median inclusion size for the different testing temperatures and materials.

A large part of fracture toughness scatter in the transition region is related to the inhomogeneous distribution of the microstructural features contributing to cleavage fracture. In the preceding section, a linear relationship between the K_{J_C} versus $\sqrt{1/d_i}$ was found. So, it can be discovered what portion of the scatter in the transition region comes from the difference in triggering inclusion size. From the linear relationship between the K_{J_C} versus $\sqrt{1/d_i}$ in Fig. 10, we normalized the K_{J_C} values by the inclusion size with the following equation:

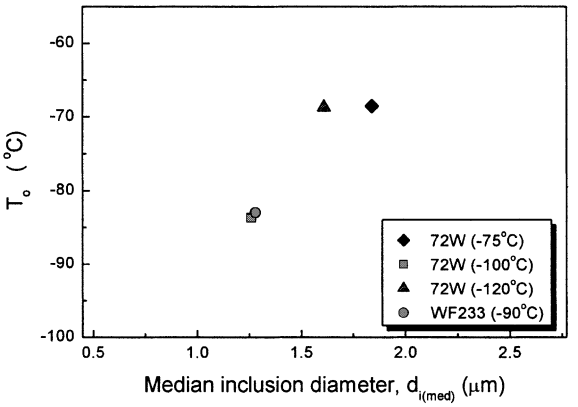

Fig. 12. A relationship between median inclusion size at trigger point and T_0 value adjusted to 1T-CT test specimen.

$$K^{i}_{J_C(1T)} = K_{J_C(1T)} + A(d^{-1/2}_{i(\mathrm{med})} - d^{-1/2}_{i}),$$

where $K^{i}_{J_C(1T)}$ = the fracture toughness normalized by the triggering inclusion factor, $K_{J_C(1T)} = Ad_i^{-1/2} + b$, $b = K_{J_C(1T)}$ where $d_i = 0$, d_i = inclusion diameter at trigger point, $d_{i(\mathrm{med})}$ = median inclusion diameter at trigger point.

The $K^{i}_{J_C(1T)}$ data set in the same temperature implies the inherent scatter range when the same inclusion size is assumed in all specimens. Fig. 13 shows the deviation of the $K^{i}_{J_C(1T)}$ values from the median values at respective temperatures. The bounding lines are from the reported large amount of data sets [5]. The width of the deviation

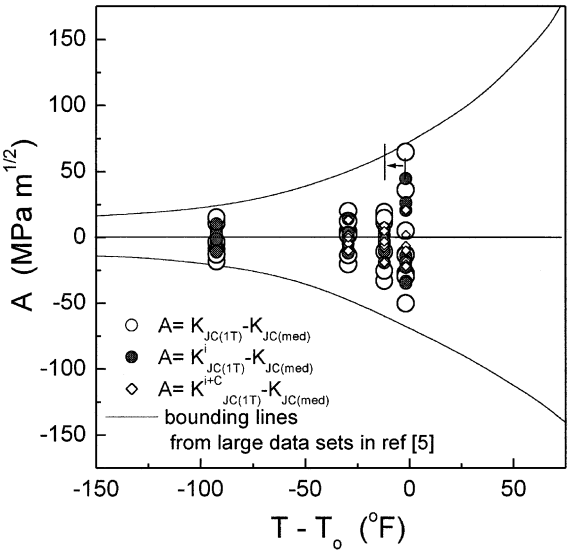

Fig. 13. The change of the fracture toughness data scatter from the median toughness values with a modification by the contribution of the inclusions which trigger a brittle fracture and induce a ductile crack growth.

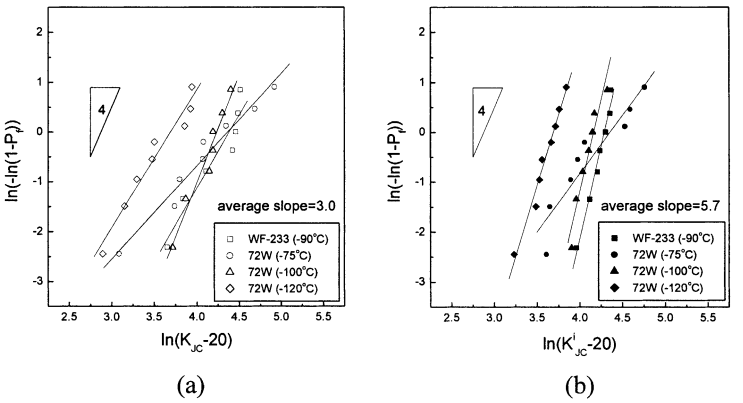

Fig. 14. Weibull plots of the fracture toughness data before (a) and after (b) the normalization by the triggering inclusion size.

becomes about 35% smaller than that before normalization and the rate of width reduction is not so different with temperature. Fig. 14 shows the weibull plots of these normalized fracture toughness values. The Weibull slopes become steeper by the normalization, which means smaller scatter and higher uniformity of the fracture toughness data in the transition region.

The inclusion can also affect the fracture toughness scatter in the transition region through promoting stable crack growth before brittle fracture initiation (Fig. 15). Stable crack growth by coalescence of the voids formed at the inclusions relaxes the applied stress in the crack-tip region and delays the stress to exceed local cleavage fracture stress of the material. It inevitably increases the measured fracture toughness value and induces fracture toughness scatter. Table 3 shows the amount of stable crack length (Δa) at the various testing temperatures. Some experimental data reported [20] supported the relation of $J_c \propto \Delta a$ or $K_{J_C} \propto (\Delta a)^{1/2}$. We normalized the $K^i_{J_{C(1T)}}$ by the stable crack length with the following equation

$$K^{i+c}_{J_{C(1T)}} = K^i_{J_{C(1T)}} + P\left((\Delta a)^{1/2}_{\text{med}} - (\Delta a)^{1/2}\right),$$

where, $K^{i+c}_{J_{C(1T)}}$ = the fracture toughness normalized by both the triggering inclusion size and stable crack length, $K^i_{J_{C(1T)}} = P(\Delta a)^{1/2} + q$.

Fig. 13 also shows the fracture toughness data normalized by both the inclusion size at the trigger point and stable crack length for the two welds. The scatter becomes smaller at -75 °C in 72W weld, but is little affected at the lower temperatures. This is reasonable because the stable crack growth becomes important with rising temperature.

A series of these normalization processes for the fracture toughness data by the microstructural factors would minimize the data scatter in the transition region. Of course, the scatter from the testing variables such as specimen dimension and fatigue pre-crack must be unavoidable. Nevertheless, knowledge about the relative contribution of the metallurgical variables on the toughness data scatter is important in understanding the fracture properties specific to the materials and in

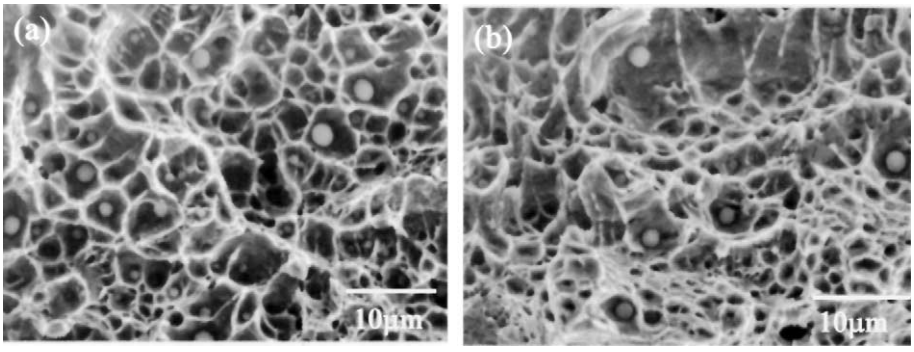

Fig. 15. Initial ductile regions on the fracture surfaces of the tested PCVN specimens of the WF-233 and 72W welds tested at -75 °C: (a) WF-233 weld and (b) 72W weld.

Table 3
The amount of stable crack growth for the two welds

Welds	Temperature (°C)	$K_{J_C(1T)}$ (MPa m$^{1/2}$)	Δa (μm)
72W	−100	86.2	5
		61.1	5
		101.7	35
		67.9	3
		86.1	24
		93.3	20
		83.3	1
	−75	97.0	33
		41.9	1
		64.7	4
		79.0	25
		78.5	10
		128.1	77
		156.8	150
		62.2	10
WF-233	−90	108.5	75
		58.6	1
		103.2	60
		66.4	5
		80.8	25
		110.9	40
		106.4	50

further developing the materials that have superior fracture properties.

6. Comparison of the two welds with different inclusion density

Comparing the two welds at testing temperatures of −100 °C for 72W and −90 °C for WF-233, the T_0 values are quite similar (Table 2). This is consistent with the similarity in the measured triggering inclusion size in the two welds. However, the total inclusion density in the two welds is different especially for the small inclusions as shown in Fig. 7. Regarding this, it is found that the triggering inclusion size was not influenced by the density difference of small inclusions. This may beexplained in terms of the critical distance or volume for fracture in front of the crack-tip as referred to in the previous section. According to the weakest-link theory governing brittle fracture and the observation in this work, fracture toughness is determined by only one inclusion to satisfy the fracture condition. If the critical volume for fracture were large enough to contain the inclusions of a certain size to initiate cleavage fracture, different inclusion density in that volume in the two welds may be not important any more. In Fig. 7, the density difference in the two welds is large for small inclusions while it becomes similar for inclusions greater than 1.5 μm. So, it is supposed that the critical distance (or volume) in the welds is related to the spacing of the inclusions greater than about 1.5 μm. But, it is still uncertain whether the critical distance quantitatively corresponds with the inclusion spacing. Because the other factors such as grain size containing the triggering inclusion and the presence of defects adjacent to the triggering inclusion can affect cleavage initiation at inclusion, the real critical distance may be several times greater than the inclusion spacing only regarding size. This idea needs further work in the future as mentioned in the preceding section.

7. Conclusions

The fracture toughness of two high copper RPV welds having low USE was evaluated in accordance with the master curve method of ASTM E1921 and the resultant data was correlated to the metallurgical factors involved in the brittle fracture initiation to provide a metallurgical-based understanding of the master curve. The conclusions are as follows.

A key microstructural factor controlling cleavage initiation in Linde 80 weld and its simulated weld was the non-metallic inclusion of the Mn–Si–Al type containing O and S.

The measured K_{J_C} was inversely proportional to the square root of the inclusion diameter at the trigger point. With the assumption of a constant triggering inclusion size, the newly determined median K_{J_C} values which correspond to the median triggering inclusion diameter of all tested specimens showed smaller deviation from the master curve than the experimental median K_{J_C} values. This suggests that the master curve is on the premise of a constant dimension of a key microstructural factor in a material regardless of the testing temperature.

The inclusion size at the trigger point played an important role in the absolute position of the master curve with temperature and the consequent T_0 value. Furthermore, a substantial portion of the data scatter in the transition region came from the difference in the triggering inclusion size and the stable crack growth before brittle fracture promoted by the inclusions.

Acknowledgements

This work has been carried out as a part of the Reactor Pressure Boundary Materials Project under the Nuclear R&D Program by MOST in South Korea. The 72W weld material was supplied by the MPC Cooperative test program.

References

[1] K. Wallin, Eng. Fract. Mech. 19 (1984) 1085.
[2] K. Wallin, Eng. Fract. Mech. 22 (1985) 149.

[3] M.A. Sokolov, R.K. Nanstad, Effects of Radiation on Materials: 18th International Symposium, ASTM STP 1325, American Society for Testing and Materials, West Conshohocken, PA, 1999, p. 167.
[4] M.A. Sokolov, D.E. McCabe, Y.A. Davidov, R.K. Nanstad, Small Specimen Test Techniques, ASTM STP 1329, American Society for Testing and Materials, West Conshohocken, PA, 1998, p. 238.
[5] M. Kirk, R. Lott, C. Kim, W. Server, ASME/JSME Pressure Vessel and Piping Symposium, San Diego, CA, 1998.
[6] K. Wallin, Int. J. Press. Ves. Pip. 55 (1993) 61.
[7] K. Willin, T. Saario, K. Torronen, Met. Sci. 18 (1984) 13.
[8] M. Kirk, M.A.E. Natishan, M. Wagenhofer, ASTM STP 1406, American Society for Testing and Materials, Philadelphia, PA, 2001.
[9] M. Natishan, M. Kirk, Proceedings of the 1999 ASME Pressure Vessel and Piping Conference, ASME, New York, July, 1999.
[10] M. Natishan, M. Wagenhofer, M. Kirk, ASTM STP 1389, American Society for Testing and Materials, Philadelphia, PA, 1999.
[11] R.O. Ritchie, J.F. Knott, J.R. Rice, J. Mech. Phys. Solids 21 (1973) 395.
[12] F.M. Beremin, Metall. Trans. 14A (1983) 2277.
[13] J.H. Chen, G.Z. Wang, H. Ma, Metall. Trans. 21A (1990) 321.
[14] A.W. Thompson, J.F. Knott, Metall. Trans. 24A (1993) 523.
[15] K.R. Lawless, W.A. Pavinich, A.L. Lowe Jr., in: F.A. Garner, C.H. Henager Jr., N. Igata (Eds.), Influence of Radiation on Material Properties: 13th International Symposium, ASTM STP 956, American Society for Testing and Materials, Philadelphia, PA, 1987, p. 321.
[16] W.A. Lawless, A.L. Lowe Jr., in: R.E. Stoller, A.S. Kumar, D.S. Gelles (Eds.), Effects of Radiation on Materials: 15th International Symposium, ASTM STP 1125, American Society for Testing and Materials, Philadelphia, PA, 1992, p. 186.
[17] G.R. Odette, K. Edsinger, G.E. Lucas, E. Donahue, in: Small Specimen Testing Techniques, ASTM STP 1329, American Society for Testing and Materials, West Conshohocken, PA, 1998, p. 298.
[18] G.R. Odette, E. Donahue, G.E. Lucas, J.W. Sheckherd, DOE/ER-0313/20, 1996, p. 11.
[19] E. Donahue, G.R. Odette, G.E. Lucas, DOE/ER-0313/27, 2000, p. 9.
[20] J. Watanabe, T. Iwadate, Y. Tanaka, T. Yokobori, K. Ando, Eng. Fract. Mech. (1987) 589.